Applied Catalysis B: Environmental 209 (2017) 476–482

Contents lists available at ScienceDirect

Applied Catalysis B: Environmental

journal homepage: www.elsevier.com/locate/apcatb

Visible-light reduction CO_2 with dodecahedral zeolitic imidazolate framework ZIF-67 as an efficient co-catalyst

Jiani Qin, Sibo Wang, Xinchen Wang*

State Key Laboratory of Photocatalysis on Energy and Environment, College of Chemistry, Fuzhou University, Fuzhou 350002, PR China

ARTICLE INFO

Article history:
Received 7 January 2017
Received in revised form 1 March 2017
Accepted 2 March 2017
Available online 6 March 2017

Keywords:
ZIF-67
Heterogeneous co-catalyst
Photocatalysis
CO_2 reduction

ABSTRACT

The nanomorphology of ZIFs strongly influences or even improves chemical properties of the metal-organic materials. Nanosized rhombic dodecahedral ZIF-67 crystals were successfully synthesized through a simple co-precipitation method at room temperature, and fully characterized by XRD, FT-IR, DRS, XPS, TEM, SEM, TGA and N_2/CO_2 sorption measurements. The as-prepared ZIF-67 material was applied to be an efficient heterogeneous co-catalyst for the photocatalytic CO_2 reduction by cooperating with a ruthenium-based dye as a photosensitizer under mild reaction conditions. Under the optimal reaction conditions, the photocatalytic CO_2 reduction system achieved a superior catalytic performance with a CO generation rate of 37.4 μmol/30 min, which was much higher than that of other types of MOFs. The carbon source of the evaluated CO was confirmed by $^{13}CO_2$ isotopic experiment. The stability and reusability of the ZIF-67 co-catalyst in the reaction system were also examined. The present work provides new insights in the developments of nanoscale ZIFs materials for photocatalytic application.

1. Introduction

The rising levels of atmospheric CO_2 and the depletion of fossil fuel reserves raise serious concerns on the problems of the global climate change and future energy supply. The conversion of CO_2 into value-added chemicals using solar energy as a green and abundant resource could simultaneously address both of the aforementioned problems, as well as provide a convenient means for energy storage [1]. The photocatalytic reduction of CO_2 with sunlight, *i.e.*, the artificial photosynthesis, is one of the most attractive routes for CO_2 utilization. Up to now, many semiconductors such as TiO_2 [2,3], CdS [4,5], $ZnGe_2O_4$ [6], $LaPO_4$ [7,8], $NaNbO_3$ [9], $SrTiO_3$ [10] and g-C_3N_4 [11–14] have been developed as efficient catalytic materials for CO_2 photofixation. However, the realized performance of photocatalytic CO_2 reduction is still unsatisfied to the requirements of practical applications. It is thus highly challenging but necessary to further enhance the photocatalytic CO_2 conversion activity to fulfill the crucial mission of solar-to-fuel transformations.

Co-catalyst modification is one of the most popular solutions to kinetically promote CO_2 photoreduction, since co-catalysts can support charge transfers in photocatalysis so as to enhance the participation of photogenerated electrons to reduce CO_2 [15,16]. On the other hand, co-catalyst can effectively lower the overpotential for CO_2 conversion reaction, resulting in the acceleration of the reaction rate [17,18]. For example, Lehn and co-workers [19] reported that using Co^{2+} as the co-catalyst, the efficiency of photocatalytic CO_2 reduction was markedly enhanced, in which the formation of $Co(bpy)_n^{2+}$ during the reaction was proposed as a major contribution for this enhancement. Tinnemans et al. [20] employed cobalt-based macrocyclic complexes as electron mediators to boost CO_2 photoconversion, and significantly improved activity and selectivity were obtained. The findings of these successful demonstrations reveal that cobalt species together with certain organic ligands are of vital importance to promote the transport of electrons and subsequently the catalytic efficiency of photocatalytic reduction of CO_2. However, the homogeneous characteristic of these cobalt cofactors is disadvantageous for their recycling use in practice. Therefore, the development of heterogeneous co-catalysts assembled by cobalt and organic motifs in well-defined metal-organic architectures is desirabled.

Metal-organic frameworks (MOFs), a novel class of hybrid functional materials fabricated by metal ions/clusters and organic ligands, characterized by orderly crystalline structures, large surface areas, uniform but tunable cavities/pores [21–23], have been found diverse applications in gas storage and separation [24–26], chemical sensors [27], biomedicine [28], optics [29], thin film

* Corresponding author.
E-mail address: xcwang@fzu.edu.cn (X. Wang).
URL: http://wanglab.fzu.edu.cn (X. Wang).

http://dx.doi.org/10.1016/j.apcatb.2017.03.018
0926-3373/

devices [30], heterogeneous catalysis [31–33], *etc.* Zeolitic imidazolate frameworks (ZIFs), as a subclass of MOFs, combine the benefits of zeolites and MOF materials [34,35], and importantly, ZIFs possess high chemical and thermal stabilities [36], as well as excellent capability for CO_2 adsorption and capture [37–40]. To date, ZIFs have been applied as catalysts or catalyst supports to catalyze different types of organic transformation reactions, such as knoevenagel condensation [41,42], cyclohexene hydrogenation [43], glycerol esterification [44], quinazolines synthesis [45] and transesterification reaction [46]. Our group have previously reported ZIF-9 as a stable co-catalyst for photochemical reduction of CO_2 by merging the advantage of porous characteristic of the MOF, for CO_2 capture, together with the catalytic function of imidazolate entities and cobalt in CO_2 reduction catalysis [33]. However, the prepared ZIF-9 shows irregular microtopography at micron level, which greatly restrict the catalytic efficiency towards the practical applications. As we all known, the nanomorphology of ZIFs strongly influences or even improves chemical properties of these metal-organic materials. And effective surface areas for catalytic performance can be enhanced by the nanomorphology of ZIFs in comparison to their macroscopic counterparts [47]. Furthermore, nanoscale metal-organic materials with well-defined and uniform sizes and morphologies could improve dispersion in aqueous media or other solvents. Cobalt based ZIFs with orderly nanotopography thus might realize the high co-catalytic efficiency for CO_2 photoreduction. ZIF-67 materials, which were formed by the self-assembly of cobalt ions and imidazolte linkers, has not been used in solar energy conversion application of CO_2 photoreduction. Herein, we are motivated to synthesize nanosized ZIF-67 as a new type of cobalt-based heterogeneous co-catalyst for the photochemical CO_2 reduction under mild conditions by cooperating with light-harvesters.

In the present work, rhombic dodecahedral ZIF-67 crystals at the nanoscale were successfully synthesized through a facile co-precipitation method at room temperature, and fully characterized by systematic physical and chemical measurements. The as-prepared ZIF-67 sample was developed as a co-catalyst to promote the photocatalytic reduction of CO_2 to CO under visible light irradiation by cooperation of dye photosensitizer $[Ru(bpy)_3]Cl_2{\cdot}6H_2O$ (bpy = 2′2-bipyridine), using triethanolamine (TEOA) as electron donor. The hybrid CO_2 conversion system efficiently operated the photochemical CO_2-to-CO conversion reaction with a CO evolution rate of 37.4 μmol/30 min. $^{13}CO_2$ isotopic experiment was performed to identify the carbon source of the generated CO. The stability and reusability of the ZIF-67 co-catalyst in the reaction system were also examined. The co-catalytic effect of ZIF-67 was also compared with other typical MOFs under the same reaction conditions.

2. Experimental

2.1. Chemicals

The chemicals used for synthesizing the material and participating in the reaction included $Co(NO_3)_2{\cdot}6H_2O$ (Alfa Aesar), 2-methylimidazole (Sigma Aldrich), $[Ru(bpy)_3]Cl_2{\cdot}6H_2O$ (Alfa Aesar), triethanolamine (TEOA) and acetonitrile (MeCN). All the chemical reagents were used without further purification. The carbon dioxide was supplied by Fuzhou Lianzhong Industrial Gases Co. Ltd (99.999%). The $^{13}CO_2$ gas, 98% enriched, was purchased from Hess chemical gas center in Beijing.

2.2. Synthesis of the material

The ZIF-67 sample was prepared following a previous reported literature [48] with a slight modification. Firstly, 2 mmol $Co(NO_3)_2{\cdot}6H_2O$ and 12 mmol 2-methylimidazole were dissolved in 30 ml and 10 ml methanol, respectively. Then, with vigorous stirring, the solution of 2-methylimidazole was added into the $Co(NO_3)_2{\cdot}6H_2O$ solution slowly. As a mixture of the two solutions, the purple precipitates were formed. After the two solutions were mixed completely, put the mixture solution at room temperature for 24 h. Finally, the purple powders were separated out by centrifugation and washed repeatedly in ethanol and then vacuum dried at 60 °C overnight. The proposed synthesis process of ZIF-67 was illustrated in Scheme 1.

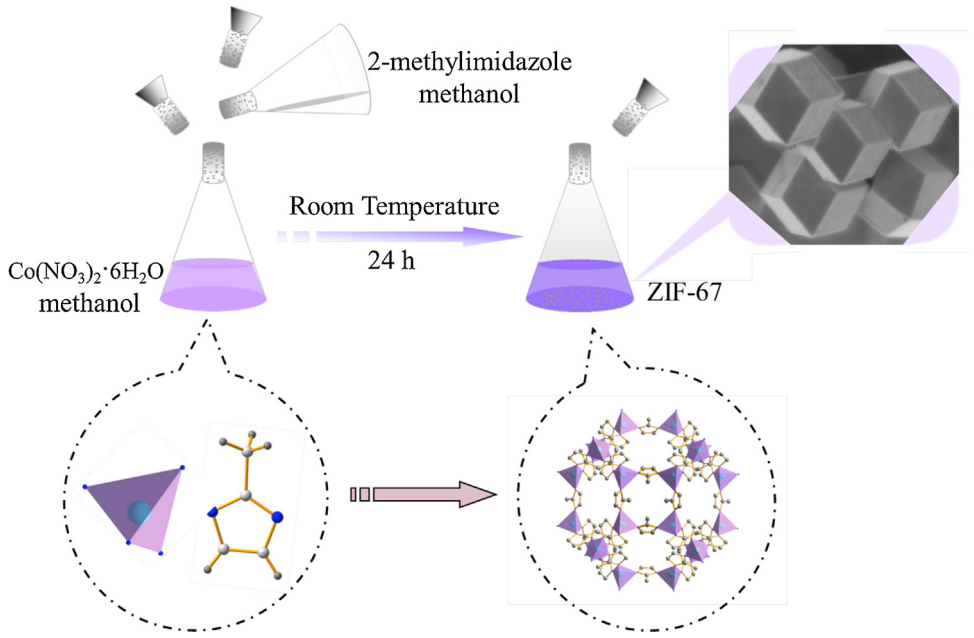

Scheme 1. The proposed synthesis process of the ZIF-67 material.

2.3. Characterization

X-ray diffraction (XRD) measurement was measured on a Bruker D8 Advance diffractometer with Cu Kα1 radiation. A Hitachi New Generation SU8010 field emission scanning electron microscope (FESEM) was employed to obtain the morphologies of the samples. Transmission electron microscope (TEM) was conducted on a JEOL model JEM 2010 EX instrument. N_2 adsorption–desorption and CO_2 adsorption isotherms were measured on a Micromeritics ASAP2020 equipment. Thermal gravimetrical analysis with a heating rate of 10 °C min^{-1} from 20 °C to 1000 °C was conducted on a Netzsch Thermoanalyzer STA 449 F3 instrument. Fourier transformed infrared (FT-IR) spectra were measured on a Nicolet Magna 670 fourier transform infrared spectrometer. A Thermo ESCALAB250 instrument with a monochromatized Al Ka line source (200 W) was used for X-ray photoelectron spectroscopy (XPS) measurements. The UV–vis diffuse reflectance spectra (DRS) of the samples were measured on a Varian Cary 500 Scan UV–vis spectrophotometer with barium sulfate as the reference. The produced gases after the reaction were analyzed on an Agilent 7820A gas chromatography equipped with a thermal conductivity detector (TCD) and a TD-1 packed column. A HP 5973 gas chromatography-mass spectrometry (GC-MS) was employed to detect the ^{13}CO generated from the $^{13}CO_2$ isotopic experiment.

2.4. Photocatalytic test

Typically, 8 mg photosensitizer $[Ru(bpy)_3]Cl_2{\cdot}6H_2O$ and 1 mg co-catalyst ZIF-67 were dispersed in a solution of triethanolamine (TEOA)/water/acetonitrile (1 mL/2 mL/3 mL). The suspension was purged with CO_2 to drive away the air in the Schlenk flask reactor, and then the reactor was full of CO_2 to conduct the reaction. With vigorous stirring, a 300 W xenon lamp with 420 nm cut-off filter was utilized as the light source and the circulation cooling water was employed to maintain the reaction temperature. After illumination for 30 min, the produced gases were analyzed by a gas chromatography.

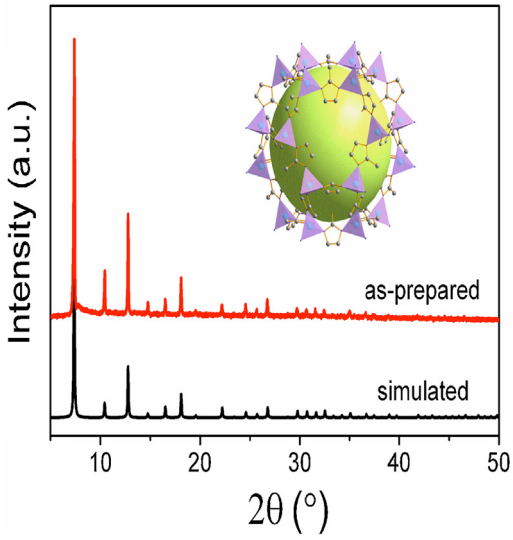

Fig. 1. XRD patterns of the as-prepared ZIF-67 sample. Inset: the sodalite topology of cubic ZIF-67.

3. Results and discussion

3.1. Characterization of the sample

XRD characterization was first carried out to investigate the crystallographic structure and phase purity of the as-prepared ZIF-67 sample. As shown in Fig. 1, the collected XRD pattern matches

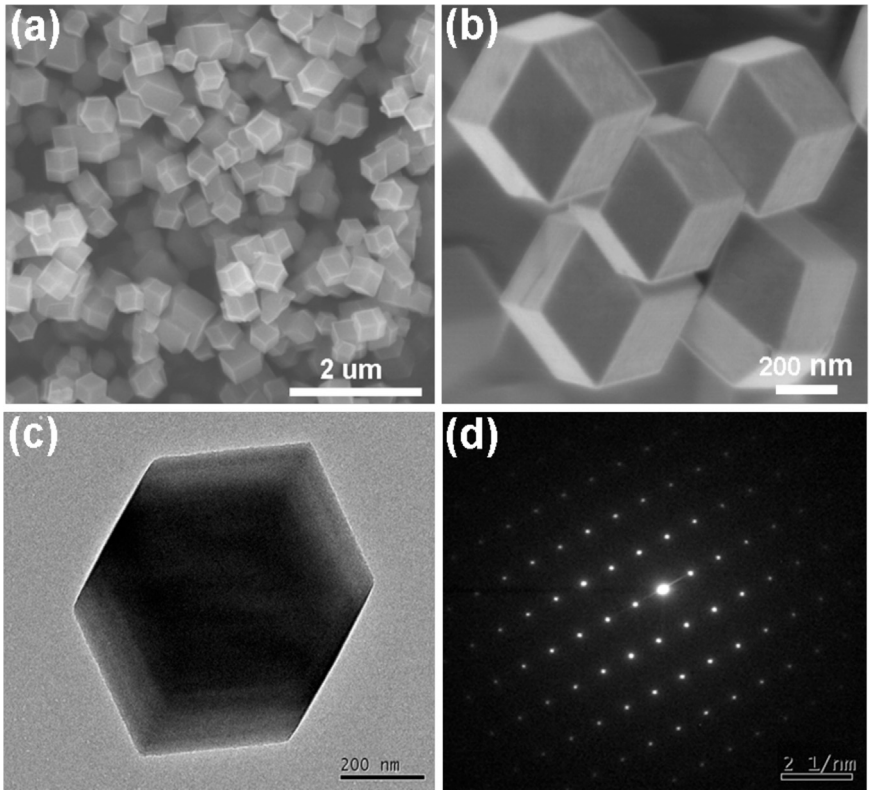

Fig. 2. SEM images (a, b), TEM image (c) and SAED pattern (d) of the ZIF-67 sample.

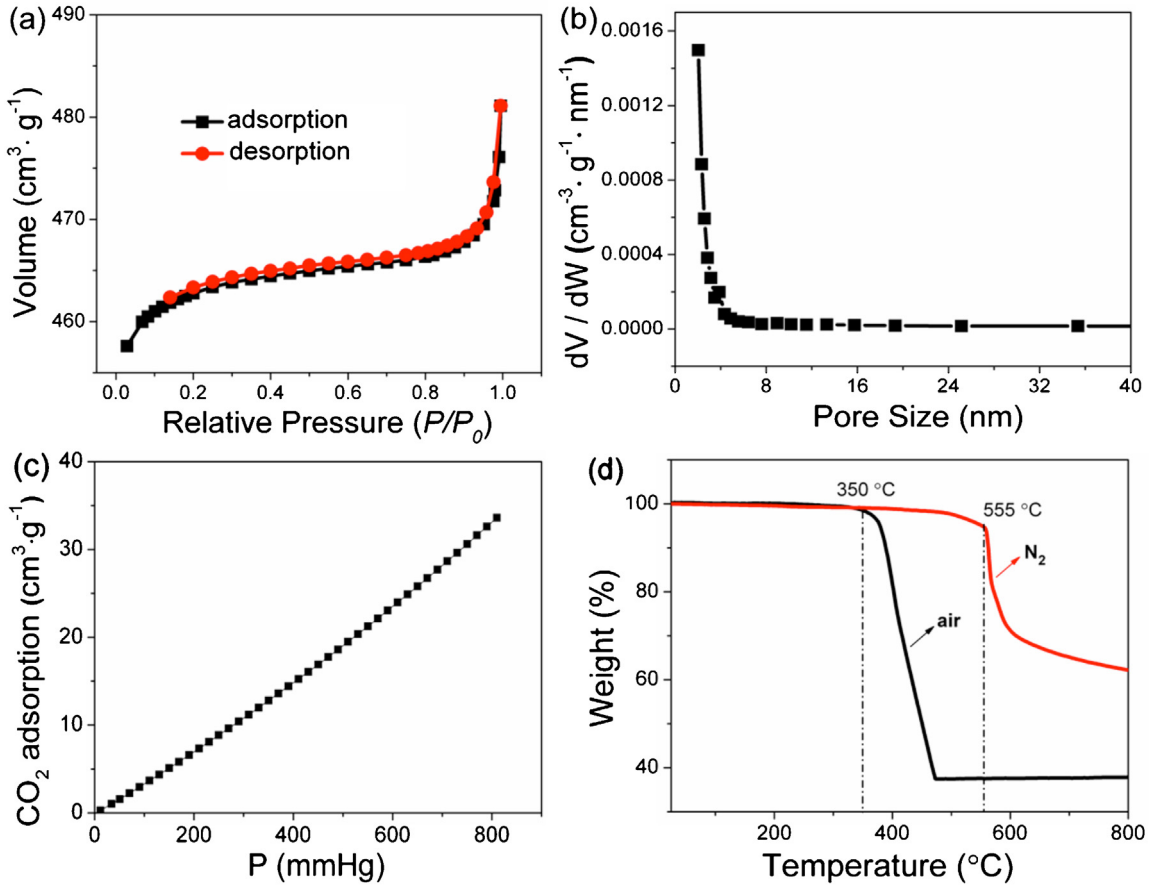

Fig. 3. (a) N_2 adsorption–desorption isotherms at 77 K, (b) the pore size distribution curve, (c) CO_2 adsorption isotherm at 273 K and (d) TGA curves of the ZIF-67 sample.

well with the simulated one, corresponding to a sodalite structure of pure cubic ZIF-67 with a SOD topology as given in the inset of Fig. 1. The sharp and strong characteristic peaks reflect the high crystallinity of the ZIF-67 material prepared with the synthesizing protocol applied.

To study the morphology and microstructure of the as-prepared ZIF-67 sample, the field emission scanning electron microscope (FESEM) was recorded on the sample. Fig. 2a is the typical low-magnification FESEM image of the ZIF-67 sample, which presents the morphology of uniform and monodispersed rhombic dodecahedral nanocrystals with a diameter of *ca.* 500 nm (Fig. 2b). The TEM image of a single dodecahedron (Fig. 2c) reveals its solid texture without discernible porosity, and the corresponding selected area electron diffraction (SAED) mirrors the perfect crystalline nature of the as-prepared ZIF-67 sample (Fig. 2d), which is consistent with the results of XRD characterization.

The BET surface area and pore structure of the prepared ZIF-67 samples were investigated using N_2 adsorption–desorption measurements. Fig. 3a shows the N_2 adsorption–desorption isotherms for ZIF-67 sample, which is categorized as type-I hysteresis loops according to the IUPAC classification, indicating the microporous characteristics of the ZIF-67 sample. The prepared sample hold a high BET surface area of 1325 $m^2\,g^{-1}$ and a high Langmuir surface area of 2023 $m^2\,g^{-1}$. The Barrett–Joyner–Halenda (BJH) pore size distribution curve (Fig. 3b) further reveals the microporous nature of the ZIF-67 sample. Such favorable microstructure with high surface area and microporous property cannot only provide the efficient transport pathways for interfacial charge carrier transferring and trapping, but also confine reactants in nanospace, which are both beneficial for photocatalytic reaction [49]. The adsorption isotherm of CO_2 for the as-prepared ZIF-67 was also measured. As shown in Fig. 3c, the ZIF-67 sample presents a high adsorption ability for CO_2 (*ca.* 34 $cm^3\,g^{-1}$), which endows a priority for heterogeneous CO_2 redox reactions. Additionally, the thermogravimetric analysis (TGA) of the ZIF-67 sample (Fig. 3d) shows the decomposition temperature located at about 350 °C in air and 555 °C in N_2, which ensure the high thermal stability of ZIF-67 in our mild reaction system.

Results of XPS measurements revealed the chemical composition and states of the as-prepared material. All the binding energies obtained in the XPS analysis were calibrated using the C 1s peak at 284.6 eV. Fig. S2 displays a full survey of ZIF-67 involving C 1s, N 1s, O 1s, and Co 2p peaks. For the high-resolution spectrum of Co 2p (Fig. 4a), two main peaks at 780.9 and 796.6 eV, separated by about 15 eV, are assigned to Co $2p_{3/2}$ and Co $2p_{1/2}$, respectively [50]. Two distinguishable satellite peaks of the Co $2p_{3/2}$ main peak are located at about 786.1 eV (Sat.a) and 791.0 eV (Sat.b) and the intensity of Sat.a is much higher than that of Sat.b. It is generally accepted that the judgement of the oxidation states of Co cations is rather difficult, and the energy gap between the Co 2p main peaks and the satellite peaks can serve as an important standard, namely that the energy gap of Co(II) cation corresponds to *ca.* 6.0 eV, while the Co(III) cation typically features the energy gap to 9–10 eV [51,52]. In this regard, Co(II) is the main form existing in the as-prepared ZIF-67 material.

To further explore the coordination situation between cobalt ions and 2-methylimidazole ligand in the as-prepared ZIF-67 sample, the characterization of ultraviolet visible diffuse reflectance spectra (UV–vis DRS) was conducted. As shown in Fig. 4b, there are three adsorption peaks at 539, 564 and 585 nm, namely the spin coupling triplet peaks, which are attributed to the $^4A_2(F) \rightarrow {}^4T_1(P)$

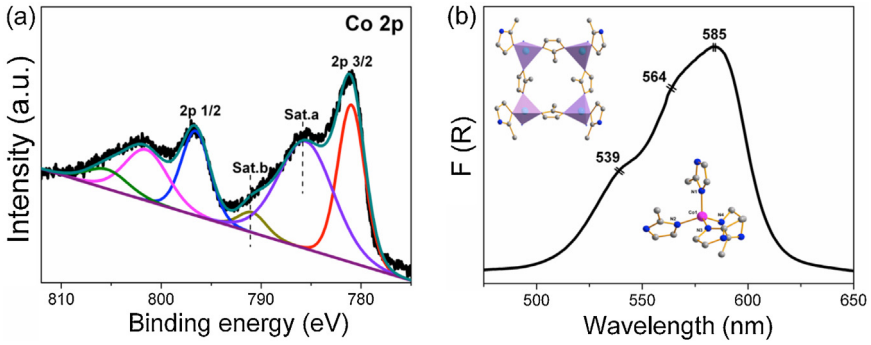

Fig. 4. (a) Co 2p high-resolution XPS and (b) UV–vis DRS spectra of the ZIF-67 sample.

transition of tetrahedral coordinated Co(II) [53,54], and it suggests no octahedral coordinated Co(II) because of no any peaks at 480 and 506 nm [55]. Combining the analysis results of XPS and DRS, it can be concluded that the cobalt species of ZIF-67 are assigned to the tetrahedral coordinated Co(II), similar to previous literature reported by others [53,54].

The surface chemical structures of the as-prepared ZIF-67 nanocrystals were studied by Fourier transformed infrared (FT-IR) characterization. The FT-IR spectra of the ligand 2-methylimidazole and the ZIF-67 material are displayed in Fig. S3. It is clearly shown that the peaks of ZIF-67 are mainly ascribed to the ligand 2-methylimidazole. The observed peaks at 600–1500 cm^{-1} are related to the stretching and bending modes of the imidazole ring, whereas the peak at 1580 cm^{-1} corresponds to the stretching mode of C=N bond in the ligand 2-methylimidazole. Moreover, the peaks at 2929 and 3135 cm^{-1} are assigned to the stretching mode of C—H from the aromatic ring and the aliphatic chain in 2-methylimidazole, respectively [56,57].

3.2. Photocatalytic activity evaluation

The catalytic property of the prepared ZIF-67 sample was evaluated in the saturated CO_2 solution with dispersed catalyst powers under visible light irradiation at mild reaction conditions. CO and H_2 are the two main reduction products. As shown in Fig. 6, with 0.1 mg ZIF-67 added, the production rates of both CO and H_2 are significantly enhanced to 37.4 and 13 μmol/30 min, respectively. The production of CO and H_2 are suppressed dramatically when ZIF-67 is absent from the system (Entry 2, Table S1), suggesting that ZIF-67 solid remarkably promotes the photocatalytic CO_2 reduction, as a heterogeneous co-catalyst.

The studies on the CO generation from the ZIF-67 catalyzed CO_2 reduction system as a function of reaction time were performed. As shown in Fig. 5, in the initial 30 min, the amount of CO increases dramatically with the prolonging of the irradiation time. After operating the reaction up to 1 h, the generation rate of the product diminishes gradually. It may be attributed to the exhaustion of the dye after long time operations under the reaction conditions [58,59]. In order to confirm this speculation, fresh dye is further added into the reaction system after 1.5 h irradiation, and the reaction proceeds again as expected. The insert graph in Fig. 5 shows that the yield of CO does not reduce in the following 1.5 h reaction, and the same phenomenon appears in the later several cycles. This result reveals the super stability of the co-catalyst ZIF-67 in such a mild system.

The effect of the adding amount of ZIF-67 for the photocatalytic CO_2 reaction was also investigated. As shown in Fig. 6, even with a tiny amount (0.05 mg) of ZIF-67 added, the chemical system achieves the CO production of 32.7 μmol and H_2 evolution of 11 μmol. When 0.1 mg ZIF-67 is included, the yield of CO reaches

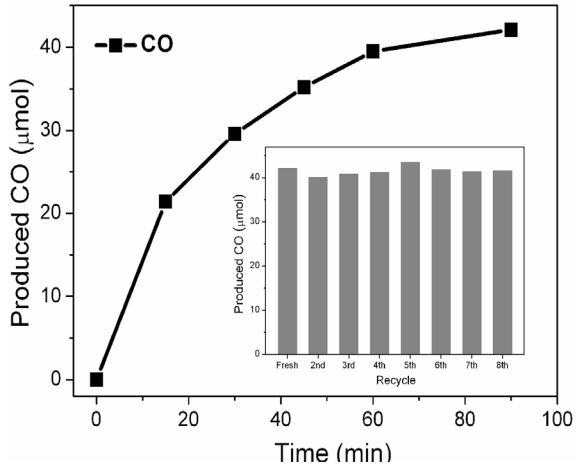

Fig. 5. Time-production plot of the CO generated from the photocatalytic CO_2 reduction system. Insert: the stability test of the CO_2 photoreduction system for eight repeated operations.

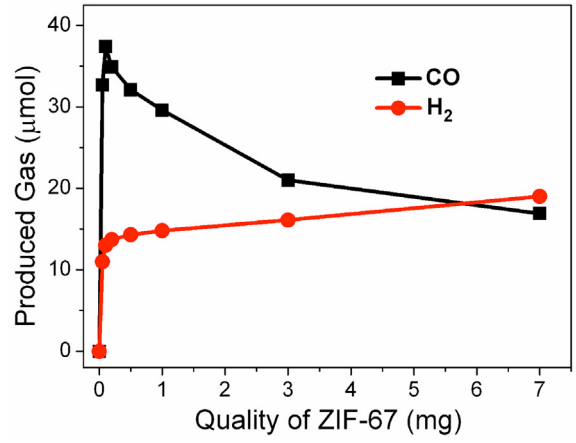

Fig. 6. The influence of the ZIF-67 amount on the evolution of CO and H_2.

a maximum value of 37.4 μmol together with a H_2 evolution of 13 μmol, giving a high catalytic turnover number (TON) of 112 and 4.7 for the chemical system, based on ZIF-67 and Ru, respectively (Fig. S4), with an apparent quantum yield (AQY) of 1.55%. Further increasing the amount of ZIF-67, the production of H_2 increases still, but the evolution of CO reduces obviously, which thus disclose the different reaction pathways for CO and H_2 formations. Based on these observations, it is concluded that the mass transfer (the adsorption and diffusion) of the reactants to the catalytic centers is the main factor that determine the reaction rate when

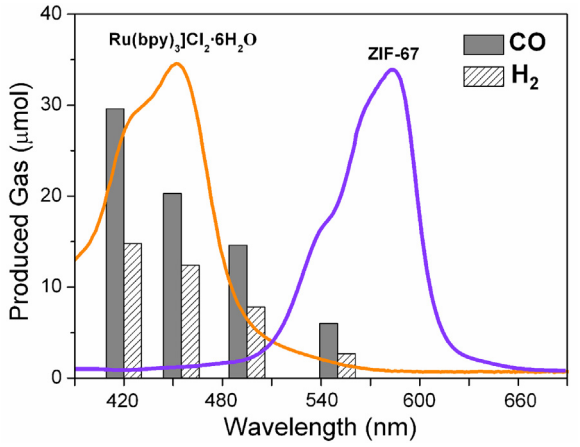

Fig. 7. The dependence of the wavelength of incident light on the evolution of CO and H_2.

Table 1
Photocatalytic CO_2 reduction performance promoted with various MOFs.

MOFs	CO/μmol	H_2/μmol	CO + H_2/μmol	Sel.CO (%)
Co-ZIF-67	29.6	14.8	44.4	66.7
Zn-ZIF-8	1.8	2.0	3.8	47.4
Cu-MOF	1.2	1.5	2.7	44.4
Zr-UIO-66-NH_2	0.9	1.2	2.1	42.9
Fe-MIL-101-NH_2	4.7	2.1	6.8	69.1

the co-catalyst is less than 0.1 mg in the catalytic system. While the co-catalyst is more than 0.1 mg, it is the electron-transfer kinetics that largely limits the reaction rate [60].

The photocatalytic performance of such a hybrid system was evaluated under light irradiation with different incident wavelength. As presented in Fig. 7, the trend of the products is coincident with the light-absorbed spectrum of the $[Ru(bpy)_3]Cl_2·6H_2O$ photosensitizer, rather than that of the ZIF-67 material. This result suggests that the CO_2 photoreduction reaction is indeed motivated by the photoexcitation of dye photosensitizer, generating excited electrons to implement tandem redox reactions, wherein the ZIF-67 co-catalyst effectively mediates the electron transport to reduce the pre-absorbed CO_2 molecules to CO.

To highlight the superior function of the cobalt species spatially linked together by imidazolate motifs in ZIF-67 in promoting CO_2 conversion catalysis, we further synthesized the ZIF-8 material using the same ligand (2-methylimidazole) and zinc ions as the precursors, and the catalytic performance of ZIF-8 for boosting CO_2 reduction reaction was evaluated. As listed in Table 1, when ZIF-8 is utilized as a co-catalyst, no prominent co-catalytic effect is observed as compared to the cocatalyst-free system (Entry 2, Table S1). Additionally, some other typical MOFs (*e.g.* Cu-HKUST-1, Zr-UiO-66-NH_2, Fe-MIL-101-NH_2) are also prepared and examined as co-catalysts for the photocatalytic CO_2 reduction system, but the CO_2-to-CO reaction is not evidently supported. All these results underline that the cobalt species of ZIF-67 are essentially indispensable for promoting electron transport and then the CO_2 photoreduction catalysis in the current system.

The flat band potential of ZIF-67 was determined to be *ca.* −0.73 V (*vs.* NHE, pH 7.0) (Fig. S5), which ensured its suitable redox ability to accept the excited electrons from the photosensitizer to operate CO_2-to-CO transformation [61,62]. The mechanism of the CO_2 photoreduction reaction was proposed as follows, under visible light irradiation, electrons photoinduced by the photosensitizer Ru-dye transferred to the ZIF-67 cocatalyst, and then the CO_2 molecules absorbed on ZIF-67 surface were reduced into CO. Meanwhile, the protons presented in the system could also be reduced by the excited electrons and produced H_2. The excited state of the Ru-dye was quenched by TEOA serving as the sacrificial electron donor.

A series of blank experiments were performed to demonstrate the essential of all components for the photoreduction of CO_2 reaction (Table S1). No CO or H_2 produces either in the dark (Entry 4, Table S1) or in the absence of dye (Entry 3, Table S1), indicating that the CO_2 reduction reaction is driven by visible light excitation of the photosensitizer. When the catalytic system is manipulated in Ar atmosphere (Entry 5, Table S1) under otherwise identical conditions, no any CO is detected, suggesting that the formed CO is originated from the reactant CO_2, not the carbon-sources in the reaction system. This is further confirmed by ^{13}C-labelled isotropic experiment under the identical photoreaction conditions. As shown in Fig. 8, after reaction for 30 min, the peak at 3.3 min with the m/z value of 29 in the results of GC-MS analysis is assigned to ^{13}CO, validating that the carbon origin of the generated CO is the CO_2 feedstock.

4. Conclusion

The rhombic dodecahedral microporous crystalline ZIF-67 was successfully synthesized through a simple co-precipitation method at the room temperature. The as-prepared zeolite imidazole framework ZIF-67 was used as a novel and efficient heterogeneous cobalt-based co-catalyst for the photocatalytic CO_2 reduction reaction. Under the optimal conditions, a high TON of 112 for the photocatalytic CO_2 reduction system were achieved after 30 min illumination. The $^{13}CO_2$ isotropic experiments confirmed that the produced CO was originated from CO_2. Intergrading the excellent electron-mediating function of cobalt species spatially confined by

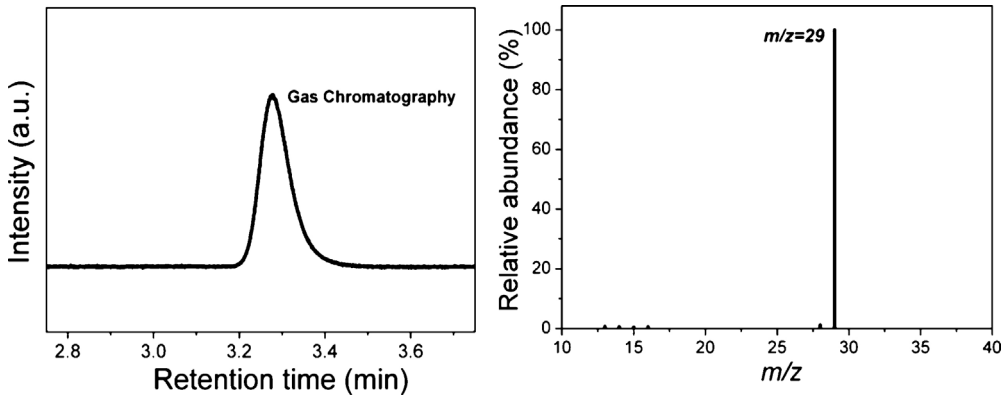

Fig. 8. Gas chromatography and mass spectra (m/z = 29) analyses of the carbon source of the generated CO in the photochemical reduction of $^{13}CO_2$.

imidazolate motifs in the heterogeneous crystalline scaffolds of the MOFs, the ZIF-67 co-catalyst presented superb promotional effect for CO_2 photoreduction catalysis than other typical MOFs. Furthermore, the ZIF-67 sample showed superior activity stability. This work may bring some insights into the target-directed design of highly efficient catalysts/co-catalysts assembled from catalytically active metals with functional organic ligands for CO_2 photofixation and artificial photosynthesis.

Acknowledgement

This work is financially supported by the National Basic Research Program of China (2013CB632405), the National Natural Science Foundation of China (21425309 and 2161101090), the National Key Technologies R&D Program of China (2014BAC13B03), the Specialized Research Fund for the Doctoral Program of Higher Education (20133514110003) and the 111 project.

Appendix A. Supplementary data

Supplementary data associated with this article can be found, in the online version, at http://dx.doi.org/10.1016/j.apcatb.2017.03.018.

References

[1] S.N. Habisreutinger, L. Schmidt-Mende, J.K. Stolarczyk, Angew. Chem. Int. Ed. 52 (2013) 7372–7408.
[2] J. Yu, J. Low, W. Xiao, P. Zhou, M. Jaroniec, J. Am. Chem. Soc. 136 (2014) 8839–8842.
[3] L. Yuan, C. Han, M. Pagliaro, Y.J. Xu, J. Phys. Chem. C 120 (2016) 265–273.
[4] S. Wang, X. Wang, Appl. Catal. B: Environ. 162 (2015) 494–500.
[5] Z. Zhu, J. Qin, M. Jiang, Z. Ding, Y. Hou, Appl. Surf. Sci. 391, Part BI (2017) 572–579.
[6] Q. Liu, Y. Zhou, J. Kou, X. Chen, Z. Tian, J. Gao, S. Yan, Z. Zou, J. Am. Chem. Soc. 132 (2010) 14385–14387.
[7] B. Pan, S. Luo, W. Su, X. Wang, Appl. Catal. B: Environ. 168 (2015) 458–464.
[8] B. Pan, Y. Zhou, W. Su, X. Wang, Nano Res. 10 (2017) 534–545.
[9] P. Li, S. Ouyang, G. Xi, T. Kako, J. Ye, J. Phys. Chem. C 116 (2012) 7621–7628.
[10] T. Arai, S. Sato, T. Kajino, T. Morikawa, Energy Environ. Sci. 6 (2013) 1274–1282.
[11] J. Qin, S. Wang, H. Ren, Y. Hou, X. Wang, Appl. Catal. B: Environ. 179 (2015) 1–8.
[12] J. Lin, Z. Pan, X. Wang, ACS Sustain. Chem. Eng. 2 (2013) 353–358.
[13] K. Maeda, K. Sekizawa, O. Ishitani, Chem. Commun. 49 (2013) 10127–10129.
[14] S. Wang, J. Lin, X. Wang, Phys. Chem. Chem. Phys. 16 (2014) 14656–14660.
[15] S. Wang, Y. Hou, X. Wang, ACS Appl. Mater. Interfaces 7 (2015) 4327–4335.
[16] B. Pan, Y. Zhou, W. Su, X. Wang, RSC Adv. 6 (2016) 34744–34747.
[17] J.M. Lehn, R. Ziessel, Proc. Natl. Acad. Sci. 79 (1982) 701–704.
[18] A.J. Morris, G.J. Meyer, E. Fujita, Acc. Chem. Res. 42 (2009) 1983–1994.
[19] R. Ziessel, J. Hawecker, J.M. Lehn, Helv. Chim. Acta 69 (1986) 1065–1084.
[20] A.H.A. Tinnemans, T.P.M. Koster, D.H.M.W. Thewissen, A. Mackor, Recl. Trav. Chim. Pays-Bas 103 (1984) 288–295.
[21] S.L. James, Chem. Soc. Rev. 32 (2003) 276–288.
[22] J.L.C. Rowsell, O.M. Yaghi, Microporous Mesoporous Mater. 73 (2004) 3–14.
[23] N.W. Ockwig, O. Delgado-Friedrichs, M. O'Keeffe, O.M. Yaghi, Acc. Chem. Res. 38 (2005) 176–182.
[24] K. Sumida, D.L. Rogow, J.A. Mason, T.M. McDonald, E.D. Bloch, Z.R. Herm, T.H. Bae, J.R. Long, Chem. Rev. 112 (2012) 724–781.
[25] J. Purewal, D. Liu, A. Sudik, M. Veenstra, J. Yang, S. Maurer, U. Müller, D.J. Siegel, J. Phys. Chem. C 116 (2012) 20199–20212.
[26] J.R. Li, J. Sculley, H.C. Zhou, Chem. Rev. 112 (2012) 869–932.
[27] L.E. Kreno, K. Leong, O.K. Farha, M. Allendorf, R.P. Van Duyne, J.T. Hupp, Chem. Rev. 112 (2012) 1105–1125.
[28] P. Horcajada, R. Gref, T. Baati, P.K. Allan, G. Maurin, P. Couvreur, G. Férey, R.E. Morris, C. Serre, Chem. Rev. 112 (2012) 1232–1268.
[29] C. Wang, T. Zhang, W. Lin, Chem. Rev. 112 (2012) 1084–1104.
[30] A. Bétard, R.A. Fischer, Chem. Rev. 112 (2012) 1055–1083.
[31] Y. Fu, D. Sun, Y. Chen, R. Huang, Z. Ding, X. Fu, Z. Li, Angew. Chem. 124 (2012) 3420–3423.
[32] S. Wang, X. Wang, Small 11 (2015) 3097–3112.
[33] S. Wang, W. Yao, J. Lin, Z. Ding, X. Wang, Angew. Chem. Int. Ed. 53 (2014) 1034–1038.
[34] A. Phan, C.J. Doonan, F.J. Uribe-Romo, C.B. Knobler, M. O'Keeffe, O.M. Yaghi, Acc. Chem. Res. 43 (2010) 58–67.
[35] S.R. Venna, M.A. Carreon, J. Am. Chem. Soc. 132 (2010) 76–78.
[36] K.S. Park, Z. Ni, A.P. Côté, J.Y. Choi, R. Huang, F.J. Uribe-Romo, H.K. Chae, M. O'Keeffe, O.M. Yaghi, Proc. Natl. Acad. Sci. 103 (2006) 10186–10191.
[37] B. Wang, A.P. Cote, H. Furukawa, M. O/'Keeffe, O.M. Yaghi, Nature 453 (2008) 207–211.
[38] D. Liu, C. Zheng, Q. Yang, C. Zhong, J. Phys. Chem. C 113 (2009) 5004–5009.
[39] S. Wang, X. Wang, Angew. Chem. Int. Ed. 55 (2016) 2308–2320.
[40] R. Banerjee, A. Phan, B. Wang, C. Knobler, H. Furukawa, M. O'Keeffe, O.M. Yaghi, Science 319 (2008) 939–943.
[41] U.P.N. Tran, K.K.A. Le, N.T.S. Phan, ACS Catal. 1 (2011) 120–127.
[42] L.T.L. Nguyen, K.K.A. Le, H.X. Truong, N.T.S. Phan, Catal. Sci. Technol. 2 (2012) 521–528.
[43] C.H. Kuo, Y. Tang, L.Y. Chou, B.T. Sneed, C.N. Brodsky, Z. Zhao, C.K. Tsung, J. Am. Chem. Soc. 134 (2012) 14345–14348.
[44] L.H. Wee, T. Lescouet, J. Ethiraj, F. Bonino, R. Vidruk, E. Garrier, D. Packet, S. Bordiga, D. Farrusseng, M. Herskowitz, J.A. Martens, ChemCatChem 5 (2013) 3562–3566.
[45] T. Truong, T.M. Hoang, C.K. Nguyen, Q.T. Huynh, N.T. Phan, RSC Adv. 5 (2015) 24769–24776.
[46] C. Chizallet, S. Lazare, D. Bazer-Bachi, F. Bonnier, V. Lecocq, E. Soyer, A.A. Quoineaud, N. Bats, J. Am. Chem. Soc. 132 (2010) 12365–12377.
[47] Y. Luan, N. Zheng, Y. Qi, J. Tang, G. Wang, Catal. Sci. Technol. 4 (2014) 925–929.
[48] R. Wu, X. Qian, K. Zhou, J. Wei, J. Lou, P.M. Ajayan, ACS Nano 8 (2014) 6297–6303.
[49] J. Yu, L. Qi, M. Jaroniec, J. Phys. Chem. C 114 (2010) 13118–13125.
[50] W. Wei, W. Chen, D.G. Ivey, Chem. Mater. 20 (2008) 1941–1947.
[51] D. Barreca, C. Massignan, S. Daolio, M. Fabrizio, C. Piccirillo, L. Armelao, E. Tondello, Chem. Mater. 13 (2001) 588–593.
[52] D.G. Castner, P.R. Watson, I.Y. Chan, J. Phys. Chem. 93 (1989) 3188–3194.
[53] H. Li, H. Ma, X. Wang, J. Gao, C. Chen, S. Shi, M. Qu, N. Feng, J. Xu, J. Energy Chem. 23 (2014) 742–746.
[54] J.P. Lourenço, M.F. Ribeiro, C. Borges, J. Rocha, B. Onida, E. Garrone, Z. Gabelica, Microporous Mesoporous Mater. 38 (2000) 267–278.
[55] J. El Haskouri, S. Cabrera, C.J. Gómez-García, C. Guillem, J. Latorre, A. Beltrán, D. Beltrán, M.D. Marcos, P. Amorós, Chem. Mater. 16 (2004) 2805–2813.
[56] K.Y.A. Lin, H.A. Chang, J. Taiwan Inst. Chem. Eng. 53 (2015) 40–45.
[57] A.F. Gross, E. Sherman, J.J. Vajo, Dalton Trans. 41 (2012) 5458–5460.
[58] J.M. Lehn, R. Ziessel, J. Organomet. Chem. 382 (1990) 157–173.
[59] S. Wang, Z. Ding, X. Wang, Chem. Commun. 51 (2015) 1517–1519.
[60] T. Maschmeyer, M. Che, Angew. Chem. Int. Ed. 49 (2010) 1536–1539.
[61] K. Kalyanasundaram, Coord. Chem. Rev. 46 (1982) 159–244.
[62] J. Schneider, H. Jia, J.T. Muckerman, E. Fujita, Chem. Soc. Rev. 41 (2012) 2036–2051.